Fe NANORODS SYNTHESIZED BY HIGH-ENERGY BALL MILLING AND SUBSEQUENT ANNEALING

J. Chihuaque[a], C. Patiño-Carachure[c], R.Pérez[b], R. Esparza[b] G. Rosas[c]*

[a]Instituto Tecnológico Superior de Irapuato Carr. Irapuato-Silao Km 12.5 P.O. Box 36821, Irapuato, Gto., México.

[b]Centro de Física Aplicada y Tecnnología Avanzada, UNAM campus Juriquilla, Boulevard Juriquilla 3001,76230 Queretaro, Qro., México.

[c]Instituto de Investigaciones Metalúrgicas, UMSNH. Edificio "U". P.O. Box 52B, 58500 Morelia, Michoacán, México.

*Corresponding autor: Gerardo Rosas, e-mail: grtrejo07@yahoo.com.mx, (52443) 3223500, ext. 4032.

Recibido: Julio 2011. Aprobado: Julio 2012.
Publicado: Julio 2012.

ABSTRACT
In this investigation, the chemical and microstructural characteristics of nanostructured Fe rods produced by mechano-thermal processes have been explored. High purity Fe powder was used as the starting material. The ball milling was carried out at room temperature using a SPEX-8000 mixer/mill. The subsequent annealing experiments were conducted at 600, 800 and 1100 ºC under inert atmosphere. The structure, morphology and compositions of the powders were obtained using X-ray diffraction patterns, scanning and transmission electron microscopy.

Key words: Fe nanorods, Electron microscopy, Annealing, Molecular Simulations, High Energy Ball Milling.

NANORODILLOS DE Fe SINTETIZADOS POR MOLIENDA DE BOLAS DE ALTA ENERGÍA Y TRATAMIENTOS TÉRMICOS

RESUMEN
En este trabajo, han sido investigadas las características microestructurales y químicas de rodillos de Fe nanoestructurado producido por un proceso mecano-térmico. Se utilizaron, como materia prima, polvos de Fe de alta pureza. La molienda de bolas fue realizada a temperatura ambiente usando un molino SPEX-8000. Los experimentos de recocido fueron realizados bajo una atmósfera de gas inerte a las temperaturas de 600, 800 y 1100 ºC. La estructura, morfología y composición de los mismos fue obtenida mediante difracción de rayos X, microscopía electrónica de barrido y de trasmisión.

Palabras clave: Nanorodillos de Fe, Microscopía electrónica, recocido, simulación molecular, molienda de alta energía

INTRODUCTION

High-energy ball milling (HEBM) is a simple technique currently used to prepare different kinds of materials. In most of them the crystal size decreases gradually reaching the nanometer scale in a few hours of milling. In recent years, HEBM has also been used for the synthesis of one dimensional (1D) nanostructured materials like a nanorods and nanotubes [1-7]. The synthesis of 1D nanostructures consist to applied HEBM to obtain nanocrystal size of iron powders and subsequently a soft annealing treatment to nanostructure growth [8-9]. Through this versatile and no expensive route, different 1D nanostructure types were prepared. On the other hand, Fe nanostructured has been produced through other synthesis methods [10-12]. The magnetic properties of nanostructured iron materials have drawn special attention due to potential applications in sensors and storage devices [13-15]. Also, iron has been found to be one of the main catalytic elements for the growth of nanotubes [16-17]. In this work, we present the results obtained after applied both HEBM and thermal treatment to iron powders to produce Fe nanorods.

MAERIALS AND METHODS

Cubic Fe-BCC powder of high purity (99.99%) was used as the starting material. Ball milling was carried out at room temperature using a SPEX 8000 mixer/mill. A stainless steel container and hardened steel balls were used. The samples were prepared in argon-flushed glove box to prevent oxidation during ball milling. A ball-to-powder weight ratio of 10:1 and 30 h. of milling was employed in all experiments. The annealing experiments were carried out at 600, 800 and 1100 ºC in a nitrogen atmosphere for different periods of time 5, 10 and 25 min. Structure, morphology and composition of the powders were characterized using X-ray diffraction patterns (Siemens D5000, CuK_{α} radiation), scanning electron microscopy equipped with an energy dispersive X-Ray spectroscope (JEOL-6400) and transmission electron microscopy (FEG Philips Tecnai F20). The TEM observations were carried out using powder samples deposited on carbon coated copper grids.

RESULTS AND DISCUSSION

Figure 1a corresponds to the XRD pattern of the sample milled during 30 h. Typical broader Fe reflections are observed as result of small crystal sizes and internal strain. Figure 1b corresponds to XRD pattern from a specimen annealed at 600 ºC for 25 min. With an increase of temperature, the broaden XRD peak transforms to sharp diffraction peaks. However, it is observed that the peak of iron grown over a broadened peak, which are indicating the partial amorphous character of the material.

Figure 2a shows a bright-field TEM image with its corresponding FFT pattern of the Fe powders after 30 h of milling. This image is confirmed that some regions of the specimen have an amorphous-like morphology. The FFT pattern inset confirms the amorphous nature of these particles. The chemical analysis in Figure 2b only illustrate iron element. However, Figure 2c, shows a bright field image of a 600 ºC annealed specimen. This image shows a crystalline tubular region embedded in an amorphous matrix. A FFT filtered image displayed in the inset show lattice-fringes of the tubular specimen. The dimensions of this nanostructure are approximately 150 nm long and 22 nm wide.

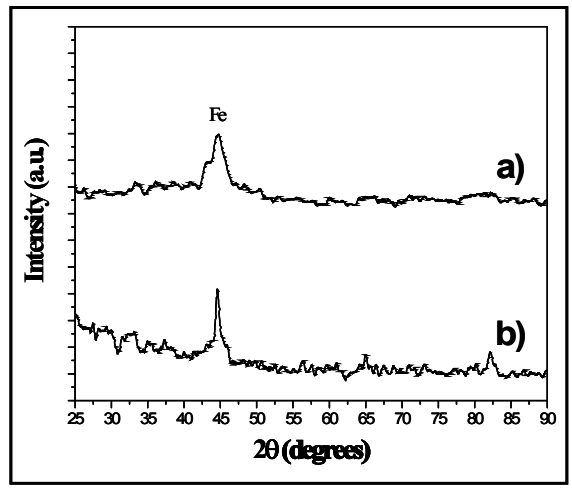

Fig. 1. X-ray diffraction patterns obtained from the iron specimens; a) after 30 h of HEBM process and b) subsequent annealing treatment at 600 ºC.

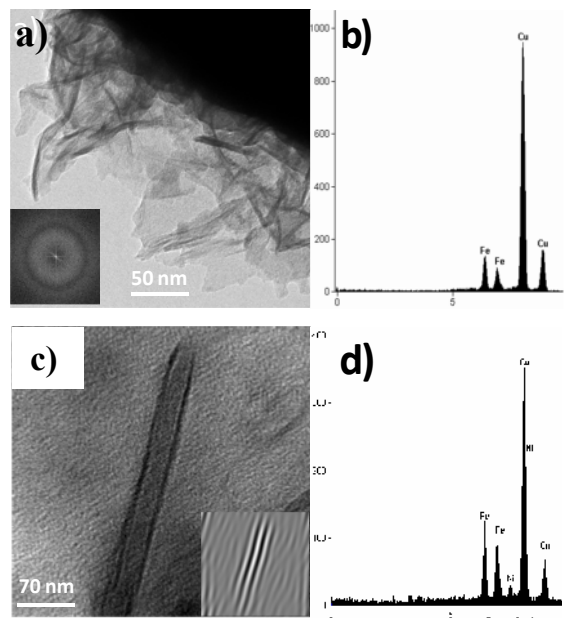

Fig. 2. a) Bright field image and the power spectrum (inset) of the Fe powders after 30 hours of milling process, b) EDS from regions of figure 2a, showing the iron presence (the Cu signal is related with the observation Cu grid), c) tubular crystalline specimen and its corresponding filtered image (inset) and d) EDS spectrum showing Fe and Ni presence.

EDS microanalysis from this region shows also the presence of Fe element (figure 2d). However, there are small amounts of Ni, this element is related with the

diffusion phenomena from the steel vial used in the milling process.

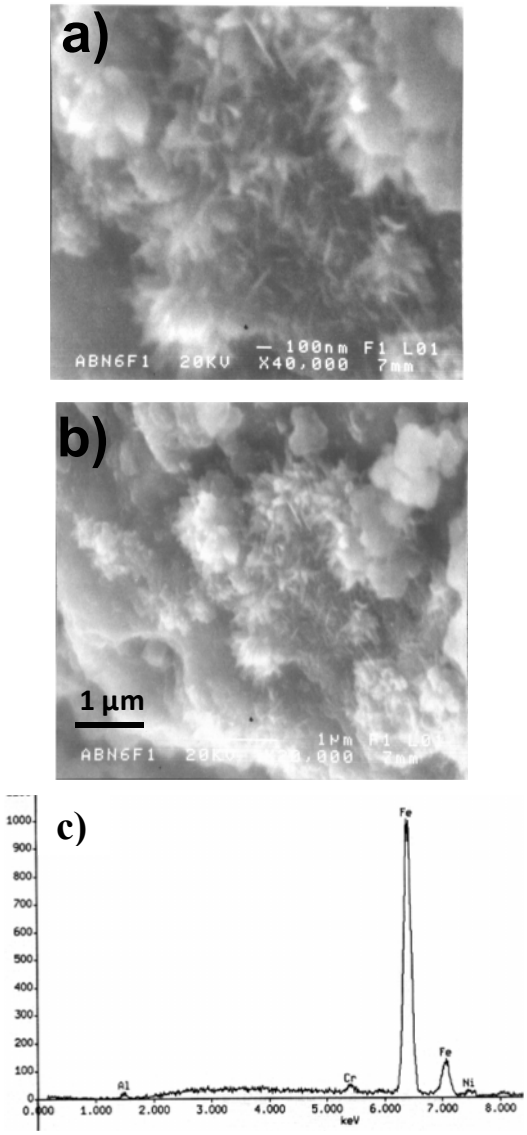

Fig. 3. a) and b), show SEM images from the annealed powder specimens. The figures show crystalline spikes growing from the material. c) EDS spectrum obtained from the spikes region showing the iron presence.

Figures 3a and b show high magnification SEM images (40,000X and 20,000X respectively) from the annealing sample at 600 ºC for 25 min. This figure clearly indicates the nanostructured spikes growing closely parallel to the surface. The EDS analysis from a dense zone of nanostructures is shown in Figure 3c. It can be observed that the composition is based on Fe with small quantities of Cr. The presence of the last element (Cr) is the result of the contamination from milling media.

As the milling media have a composition mainly based on iron, the presence of Cr in the powders also suggests iron contamination. These results are in agreement with the XRD data.

It is noteworthy that the growth of these nanostructures was only obtained for a temperature of 600 C. Above this temperature the iron nanorods decompose. Figure 4 shows bright-field TEM images of iron nanorods after the heat treatment procedure at 600 C. The nanorods have different sizes in ranges of approximately 120 and 200 nm long and 15-25 nm wide. These images show some preferred orientation growth of these iron rods, but, were generally observed that grew in several directions.

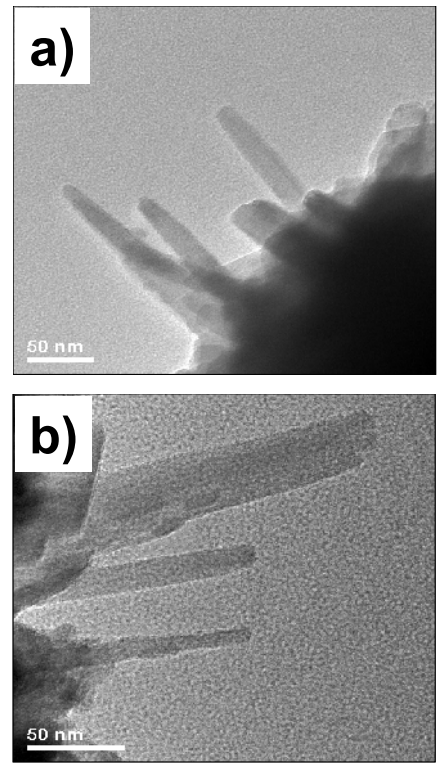

Fig. 4. Bright field images (a and b) of nanorods after the annealing procedure at 600 ºC. Their sizes are in the range of 120 to 200 nm long and 15 to 20 nm wide.

More data about the composition of the nanorods were obtained using a STEM line scan technique. Figure 5a

shows a HAADF image (High-Angle Annular Dark Field) with high bright contrast in the middle of the nanorod, this is in agreement with the iron profile, illustrated in figure 5b, where a high iron contents was obtained in the central region. Because the HAADF technique show thickness contrast the detector receives more iron counts from the central region of nanorods that elsewhere due to the cylindrical nature (the nanorod is thinner on both sides). HREM image of these nanorods is displayed in figure 6a where lattice fringes with a 0.208 nm lattice distance can be seen. This distance corresponds to the (200) interlayer spacing of the iron FCC structure. The HREM image contrast of the iron nanorod shows a surface layer where the lattice fringes ends. This layer is about 3 nm and presumably its chemical composition would be based on an iron oxide.

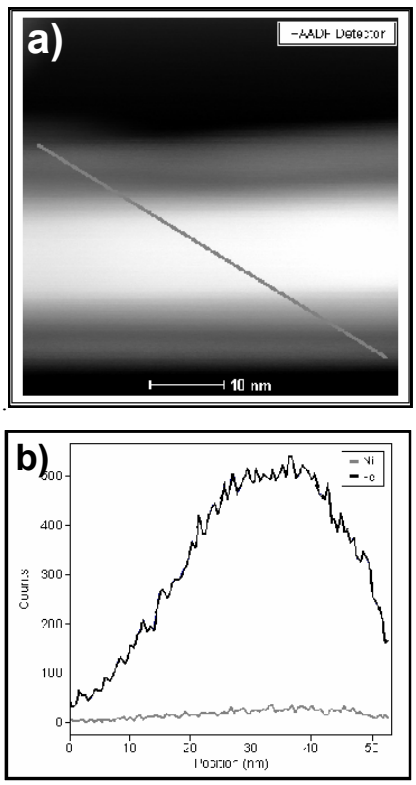

Fig. 5. a) HAADF (high angle dark field image) showing high bright contrast in the center of the nanorod. b) STEM X ray linescan from the nanorod. There is a high iron profile in the central region of the nanorod in agreement with the high angle dark field image contrast.

In order to get a qualitative insight of the HREM image contrast displayed by the iron nanorod, a theoretical simulation based on the multislice approach of the dynamical theory of electron diffraction has been carried out [16]. Figure 6b shows the supercell used for the simulation. This structure is based on a truncated FCC nanoparticle with a growing direction along the [001] axis. This structural model takes into consideration an atomic layer of oxygen stacking on the iron nanorod surface. A geometry optimization procedure was applied to this structure based on SimulaTEM software [16]. Figure 6c shows the HREM simulated image at the Scherzer's defocus This image resembles the main image contrast characteristics of the experimental HREM image (figure 6a). The simulated HREM image includes the external surface layer of the iron nanorod, suggesting that the layer is of oxide nature.

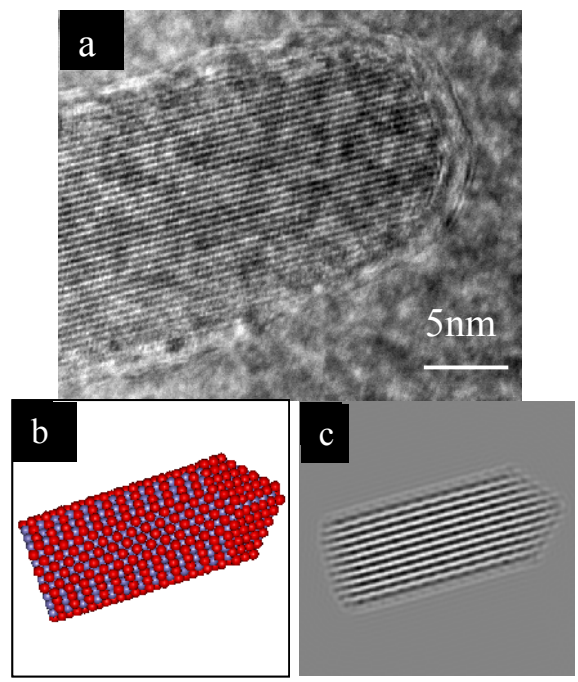

Fig. 6. a) HREM image of an iron nanorod which displays lattice fringes (0.208 nm lattice distances). The image contrast indicates the presence of an external layer of material on the nanorod surface. b) nanorod supercell used for the multislice simulation. This structural model has a stacked oxygen layer. c) HREM simulated image at the Scherzer's defocus. This image resembles the main image contrast features of the experimental nanorod HREM image.

CONCLUSIONS

Nanorods of iron were obtained with a mechanically alloyed technique, following with a subsequent annealing at 600 ºC of the obtained powders. The chemical nature of the nanorod was confirmed with EDS, high resolution X-ray linescan and also with high angle dark field images. Simulated HREM images suggest that the external layer of the nanorod is of oxide nature.

ACKNOWLEDGEMENTS

G. Rosas would like to thank the financial support received from the National Council for Science and Technology of Mexico (CONACYT) under the grant 48716-25535.

REFERENCES

[1] Muñoz J. E. , Cervantes J., Esparza R. Rosas G. (2007) "Iron nanoparticles produced by high-energy ball milling" *J. of Nanoparticle Research* 9(5): 945-950.

[2] Prasad Y. T., Manohar Y. R., Singh D. P. (2012) "Mechanical Milling: a Top Down Approach for the Synthesis of Nanomaterials and Nanocomposites" *Nanoscience and Nanotechnology* 2(3): 22-48.

[3] Rosas G., Esparza R., Liu H.B., Ascencio, J.A. Pérez R. (2007) "Mechancial alloying synthesis of carbon nanotubes in the presence of AlFe small clusters" *Mater. Lett*., 61(3):860–863.

[4] Francke M, Herman H., Wenzel R., Seifert G, Wetzig K., (2005) „Modification of carbon nanostructures by high energy ball-milling under argon and hydrogen atmosphere" *Carbon* 43(6):1204-1212.

[5] Rosas G., Esparza R., Liu H.B. Ascencio, J.A., Pérez R. (2005) "Preparation of AlFe Nanoparticles by Mechanical Alloyed Technique" *J. of Nanosci. and Nanotech.* 5(12):2133-2137.

[6] Rosas G., Sistos J., Ascencio J.A., Medina A., Pérez R., (2005) "Múltiple-walled BN nanotubes obtained with a mechanical alloying technique" *Applied Phys. A*, 80:377-380.

[7] Ayala-Sistos J., Rosas G., Esparza R. y Pérez R., (2005) "BN Nanorod Production Using Mechanical Alloying" *Adv. In Tech. Of Mat. And Mat. Proc. Journal.* (ATM) 7(2):175-180.

[8] Chen Y., Gerald J. F., Chadderton L. T., Chaffron L., (1999) "Mechanochemical Synthesis of Boron Nitride Nanotubes" *J. Metastable and Nanocrystalline Materials* 2-6:173-178.

[9] Chen Y, Lewis T. C., Fitz Gerald J., Williams J. S. (1999) "A solid-state process for formation of boron nitride nanotubes" *Appl. Phys. Lett*. 74:2960-2962.

[10] Ling T., Yu H., Liu X., Shen Z. and Zhu J. (2008) "Five-fold Twinned Nanorods of FCC Fe: Synthesis and Characterization" *Cryst. Growth Des., 8(*12):4340–4342.

[11] Qiu R., You Z. J., Cha H. G., Jung M. H., Lee J. K. and Young K. S. (2012) "One-dimensional ferromagnetic dendritic iron wire array growth by facile electrochemical deposition" *Nanoscale*, 4:1565-1567.

[12] Zhang D., Ni X., Zheng H. (2005) "Surfactant-controlled synthesis of Fe nanorods in solution" *J. Colloid Interf. Sci*., 292(2): 410–412.

[13] Hu ., Zhang Z., Zhou Q., Liu W., Li Z., Meng D. (2012) "Realignment of slanted Fe nanorods on silicon substrates by a strong magnetic field" *Nano Research* 3(6):438-443.

[14] Sia P.Z., Choi C.J., Bruck E., Klaasse J.C.P., Geng D.Y., Zhang Z.D. (2007) "Synthesis, structure and magnetic properties of iron-doped tungsten oxide nanorods" *Physica B*. 392:154–158.

[15] Clavijo-Jordan V., Kodibagkar D. V., Beeman C. S., Hann D. B., Bennett M. K. (2012) "Principles and emerging applications of nanomagnetic materials in medicine," *Nanomed Nanobiotechnol,* 4:345-365.

[16] Guo J., Wang R., Tjiu W. W., Pan J., Liu T., Synthesis of Fe (2012) "nanoparticles@graphene composites for environmental applications"

Journal of Hazardous Materials, 225–226:63–73.

[17] Lan Y., Wang Y. Ren Z.F. (2011) "Physics and applications of aligned carbon nanotubes" *Advances in Physics* 60(4):553–678.

[18] Atkinson D. J., Fortunato E. M., Dastgheib A. S., Rostam-Abadi M., Rood M. J., S. S. Kenneth, (2011) "Synthesis and characterization of iron-impregnated porous, carbon spheres prepared by ultrasonic spray pyrolysis" *Carbon*, 49:587 –598.

[19] Gómez-Rodríguez A., Beltrán del Río L. M., Herrera-Becerra R., (2010), "SimulaTEM: multislice simulations for general objects" *Ultramicroscopy*, 110 (2):95-104.